The ATP−Mg^{2+} Binding Site and Cytoplasmic Domain Interactions of Na^+,K^+-ATPase Investigated with Fe^{2+}-Catalyzed Oxidative Cleavage and Molecular Modeling†

Guy Patchornik,‡ Keith Munson,§ Rivka Goldshleger,‡ Alla Shainskaya,|| George Sachs,§ and Steven J. D. Karlish*,‡

Department of Biological Chemistry and Biological Mass Spectrometry Facility, Weizmann Institute of Science, Rehovot 76100, Israel, and Membrane Biology Laboratory, Department of Physiology, University of California at Los Angeles and VA Greater Los Angeles Healthcare System, Los Angeles, California 90073

Received June 20, 2002; Revised Manuscript Received July 29, 2002

ABSTRACT: This work utilizes Fe^{2+}-catalyzed cleavages and molecular modeling to obtain insight into conformations of cytoplasmic domains and ATP−Mg^{2+} binding sites of Na^+,K^+-ATPase. In E_1 conformations the ATP−Fe^{2+} complex mediates specific cleavages at 712VNDS (P domain) and near 440VAGDA (N domain). In E_2(K), ATP−Fe^{2+} mediates cleavages near 212TGES (A domain), near 440VAGDA, and between residues 460−490 (N domain). Cleavages at high ATP−Fe^{2+} concentrations do not support suggestions for two ATP sites. A new reagent, fluorescein−DTPA, has been synthesized. The fluorescein−DTPA−Fe^{2+} complex mediates cleavages similar to those mediated by ATP−Fe^{2+}. The data suggest the existence of N to P domain interactions in E_1Na, with bound ATP−Fe^{2+} or fluorescein−DPTA−Fe^{2+}, A−N, and A−P interactions in E_2(K), and provide testable constraints for model building. Molecular models based on the Ca^{2+}-ATPase structure are consistent with the predictions. Specifically, high-affinity ATP−Mg^{2+} binding in E_1 is explained with the N domain tilted ca. 80° toward the P domain, by comparison with well-separated N and P domains in the Ca-ATPase crystal structure. With ATP−Mg^{2+} docked, bound Mg^{2+} is close to both D710 (in 710DGVNDS) and D443 (in 440VAGDASE). D710 is known to be crucial for Mg^{2+} binding. The cleavage and modeling data imply that D443 could also be a candidate for Mg^{2+} binding. Comparison of E_1·ATP,Mg^{2+} and E_2 models suggests an explanation of the high or low ATP affinities, respectively. We propose a scheme of ATP−Mg^{2+} and Mg^{2+} binding and N, P, and A domain interactions in the different conformations of the catalytic cycle.

The Na^+,K^+-ATPase pumps 3 Na^+ and 2 K^+ ions for each ATP molecule hydrolyzed, coupling the scalar process of free energy transfer from ATP to the protein with vectorial ion transport. The kinetic mechanism of Na^+,K^+-ATPase, as of all other P-type pumps, is now largely understood (*1*, *2*). An explanation of the kinetic mechanism in terms of molecular structure is the central challenge for an understanding of energy transduction by the Na,K-pump and related P-type cation pumps.

The Na^+,K^+-ATPase, like the gastric H^+,K^+-ATPase, consists of α and β subunits with 10 and one trans-membrane segments, respectively (*3*, *4*). Renal Na^+,K^+-ATPase also contains a small γ subunit, which is a mainly kidney-specific regulator (*5*). Functional sites for ATP, Mg^{2+}, Na^+ and K^+, or ouabain reside on the α-subunit. The glycosylated β subunit stabilizes the α subunit and enables trafficking from the endoplasmic reticulum to the cell membrane (*6*, *7*). Information on structure−function relations of Na^+,K^+-ATPase (or other P2-type ATPases such as the H^+,K^+-ATPase) should be related to the 3D crystal structure of the Ca^{2+}−ATPase (*8*). Justification for use of the Ca-ATPase structure, or homology models, as a paradigm for investigating other P-type ATPase comes from the extensive sequence homologies, in the conserved cytoplasmic domains, similar topological organization, and general reaction mechanism (*9*, *10*). In addition, analysis of Na^+,K^+-ATPase by electron microscopy to 9−11 Å resolution shows similar dimensions and structural organization of the α subunit to Ca^{2+}-ATPase, while a difference in electron densities is attributed to the β subunit (*11*, *12*).

The Ca^{2+}-ATPase molecule consists of head, stalk, and membrane sectors (*8*). There are 10 trans-membrane segments in the membrane domain with two Ca^{2+} ions ligated approximately in the center of the bilayer and between transmembrane segments M4, M5, M6, and M8 in the $E_1$2Ca conformation. The stalk sector consists of the cytoplasmic extensions of the trans-membrane helices, particularly S5 and S4. The cytoplasmic sector consists of three domains, N (nucleotide binding), P (phosphorylating), and A (also referred to as the β domain). The P domain is composed of two parts (residues 330−359 and 605−737, respectively)

† This work was supported by a grant (15/00-1) from the Israel Science Foundation (S.J.D.K.) and in part by USVA and NIH Grants DK46971, 53462, 41301, and 17294 (GS).

* Corresponding author. Tel: 972 8 934 2278. Fax: 972 8 934 411. E-mail: steven.karlish@weizmann.ac.il.

‡ Department of Biological Chemistry, Weizmann Institute of Science.

§ University of California at Los Angeles and VA Greater Los Angeles Healthcare System.

|| Biological Mass Spectrometry Facility, Weizmann Institute of Science.

10.1021/bi026334d CCC: $22.00 © 2002 American Chemical Society
Published on Web 09/04/2002

located on cytoplasmic extensions of membrane helices M4 and M5 and has a Rossman fold analogous to that of L-2-haloacid dehalogenase (HAD) and related proteins with homologies to P-type pumps in conserved cytoplasmic sequences (*13*, *14*). The polypeptide from residues 360−604 exits the Rossman fold to form the N domain. The A domain consists of the N terminal residues 1−40 and the loop between M2 and M3 (residues 124−246). Comparison of the crystal structure (an $E_1 2Ca^{2+}$ conformation) with cryoelectron microscope images of Ca^{2+}-ATPase in an E_2 conformation shows that the molecular envelope of the two conformations is dramatically different (*8*, *15*, *16*). In the E_1 conformations, the N, P, and A domains are separate, while in E_2 conformations, the domains are gathered together. To account for the E_2 structure at atomic resolution, the approach has been to consider the N, P, and A as rigid domains and move them independently to fit the E_2 density profile (*8*, *16*). Throughout this paper the E_1 structure (protein database identification number 1EUL) has been compared with a recent theoretical model of the E_2 structure (protein databank identification number, 1KJU) produced by this procedure at about 6 Å resolution (*16*).

For analysis of conformational transitions and ligand binding of Na^+,K^+-ATPase or gastric H^+,K^+-ATPase, we have described the technique of specific Fe^{2+}-catalyzed oxidative cleavage (see refs *17*−*19* and a recent review, *20*; see also refs *21* and *22* for specific Cu^{2+}-catalyzed cleavages). Specific cleavages can be mediated either by bound Fe^{2+} ions or by the ATP−Fe^{2+} complex in the presence of ascorbate and hydrogen peroxide. The cleavages provide information on the spatial organization surrounding the bound Fe^{2+}, and cleavages of renal Na^+,K^+-ATPase and gastric H^+,K^+-ATPase are essentially identical (*23*). Bound Fe^{2+} ions mediate cleavages at two sites. Site 1 is composed of residues in highly conserved sequences within the P domain (369DKTGT, 710DGVNDS, 608MVTGD) and A domain (212TGES), while site 2 is located between trans-membrane segments M3 (283HFIH) and M1 (80EWVK). Site 1 exists in E_2 conformations but not in E_1 conformations. Site 2 exists in both conformations. The ATP−Fe^{2+} complex bound to the high-affinity site in the E_1 conformation mediates major cleavages in the P domain (712VNDS) and less prominent cleavages in the N domain(near 440VAGDA). Fe^{2+} ions substitute for Mg^{2+} ions in catalyzing phosphorylation and ATPase activity (*24*, *25*). Thus, the cleavage sites mediated by ATP−Fe^{2+} provide information on Mg^{2+} binding sites. Upon transition from E_1−P to the E_2−P conformation, the Fe^{2+} is tightly bound and mediates a major cleavage at 214ESE (A domain) and less prominent cleavage at 712VNDS (P domain). This change in cleavage pattern may derive from a change in Mg^{2+} ligation within these segments. It may be required for the change of reactivity from an ADP-sensitive E_1P to a water-sensitive E_2−P (*19*, *23*, *25*). One major prediction from the cleavages is that $E_1 \rightarrow E_2$ and $E_1P \rightarrow E_2P$ conformational changes are associated with large movements in the cytoplasmic domains (*17*−*19*, *23*). These inferences are consistent with the difference observed between the crystal structure of Ca^{2+}-ATPase in the $E_1{\cdot}2Ca^{2+}$ conformation (PDB ID 1EUL) or the theoretical model in the E_2 conformation (PDB ID 1KJU) (*8*, *15*, *16*). The cleavages also provides evidence for residues that are involved in the domain docking, and in binding phosphate or the γ-phosphate of ATP or Mg^{2+} ions, which is not available from the crystal structure. One conclusion from the prior work is that the changes in structure and ligand binding within the cytoplasmic sectors associated with E_1/E_2 conformational transitions are essentially similar for Na^+,K^+-ATPase, H^+,K^+-ATPase and Ca^{2+}-ATPase and presumably, therefore, for other P-type cation pumps.

The primary objective of this work has been to determine features of ATP−Mg^{2+} binding and associated N, P, and A domain interactions in E_1 and E_2 conformations that are not seen in the Ca^{2+}-ATPase structure or models, due to the absence of ATP and Mg^{2+}. The current study combines cleavages mediated by the ATP−Fe^{2+} complex and a new reagent, fluorescein−DTPA,[1] together with molecular modeling to test predictions of the cleavages. The crystal structure of Ca^{2+}-ATPase in the $E_1{\cdot}2Ca$ conformation was determined in the absence of ATP. The N and P domains are separated, but it is evident that the N and P domains must come into proximity when ATP donates its phosphate group. On the basis of our previous observations, one could predict that the cleavage points in the P (712VNDS) and N (440VAGDA) domain come into proximity when ATP−Mg^{2+} is bound (*19*, *23*). The E_2 models predict A, P, and N domains interactions, but there is little direct information on docking of A and N domains and the low-affinity ATP−Mg^{2+} binding site. Low-affinity ATP−Mg^{2+} binding to E_2K is the first step of the catalytic cycle of Na^+,K^+-ATPase in physiological conditions, and the $E_2(K) \rightarrow E_1$ transition is the major rate-limiting step (*29*, *30*). Thus, the structural basis of the different binding energies in the E_1 and E_2 conformations and the acceleration of the rate of $E_2(K) \rightarrow E_1$ by ATP [see ref *1*] are important and open questions.

A secondary objective has been to test suggestions that the Na^+,K^+-ATPase contains two coexisting ATP sites located either on the same α/β protomer or on interacting protomers (reviewed in ref *31*). Much of the evidence thought to justify this hypothesis is based on binding and labeling involving ATP analogues, containing bulky substituent groups (*32*−*35*). Experiments using substrate analogues carry the inherent risk of detecting binding properties that are features of the substituent groups themselves but are absent from the native substrate. Thus it could be informative to look at cleavages at high concentrations of the bound ATP−Fe^{2+} complex, which is a substrate of Na^+,K^+-ATPase (*24*, *25*).

EXPERIMENTAL PROCEDURES

Materials. For SDS−PAGE, all reagents were purchased from Bio-Rad. The ECL+ plus Western blotting system was from Amersham Pharmacia Biotech. All other reagents were of analytical grade. Tris (ultrapure) was from Bio Lab, Jerusalem. L-(+)-Ascorbic acid (cat. 100127) and 30% H_2O_2 (cat. 822287) were from Merck. Desferrioxamine mesylate (Desferal) (D9533), ATP$(Na)_2$ (A2383), FITC (F4274),

[1] Abbreviations: H_2O_2, hydrogen peroxide; PVDF, poly(vinylidene difluoride); DMF, dimethyl formamide; HAD, haloacid dehalogenase; FITC, fluorescein−5-isothiocyanate; Er−ITC, erythrosin−5-isothiocyanate; phosphonatase, phosphonoacetaldehyde hydrolase; AMP−PNP, 5′-adenylyl-β,γ-imidodiphosphate; fluorescein−DTPA, diethylenetriaminepentaacetic acid−1-amido-fluoresceinamine, isomer I; SERCA1, sarcoplasmic reticulum Ca-ATPase.

oligomycin (O4876), eosin Y (E6003), ouabain (O3125), and α-chymotrypsin (C4129) were from Sigma. Other reagents were of analytical grade. ATP$(Na)_2$ was converted to the Tris salt by passage through a column of Dowex-Tris. Diethylenetriaminepentaacetic dianhydride and Fluoresceinamine, isomer I were obtained from Aldrich 28,402-5, and 20,162-6, respectively.

Enzyme Preparations. Pig kidney Na^+,K^+-ATPase was prepared and assayed as described in ref *36*. The specific activity was 15−20 μmol·mg^{-1}·min^{-1}. Prior to use, membranes were washed twice and suspended in 10 mM Tris·HCl pH 7.2. FITC-labeled enzyme was prepared as described in ref *37* by incubation with 20 μM FITC, at pH 9 for 4 h at 20 °C. For comparison with Fe-cleavage fragments, the enzyme was cleaved with chymotrypsin as described in ref *18*.

Cleavage Reactions. Membranes (0.25 mg/mL protein), were suspended in the buffer containing NaCl or RbCl 100 mM respectively in lanes marked Cont. Rb or Cont·Na and other reagents, including ATP(Tris) or fluorescein−DTPA(Tris), at the indicated concentrations. The enzyme was incubated at 20 °C with freshly prepared solutions of 5−20 mM ascorbate (Tris) plus 5−10 mM H_2O_2 and 5−500 μM $FeSO_4$, premixed at 0 °C, in a total volume of 30 μL. To arrest the reaction, 20 μL of the gel sample buffer including 1 mM EDTA and 1mM Desferal was added, and samples were applied to gels.

SDS−Gel Electrophoresis and Western Blotting. Samples were applied to 1.0 mm thick 10% (34:1 acrylamide/methylene bisacrylamide) slab gels, using the tricine buffer method of Schägger and von Jagow (*38*). Gels were run overnight at 30−50 V constant voltage, and the protein was then transferred to poly(vinylidene difluoride) (PVDF), as described previously (*39*). Anti-K1012−Y1016, directed against the C-terminal sequence of the α subunit and referred to as anti-KETTY, was used to detect fragments of Na^+,K^+-ATPase. Immunoblots were developed by enhanced chemiluminescence (ECL+plus kit) using antirabbit IgG horseradish peroxidase conjugate and the protocol supplied with ECL+plus reagents from Amersham Pharmacia Biotech. Immunoblots were scanned with a Biorad imaging densitometer (GS-690) and analyzed using the Multi-analyst software.

Synthesis of Fluorescein−DTPA. To a stirred solution of 857 mg (2.4 mmole) of diethylenetriaminepentaacetic dianhydride (Aldrich 28,402−5) in 10 mL of dry DMF were added 83 mg (0.24 mmole) of fluoresceinamine and isomer I (Aldrich 20,162-6) in 0.5 mL of dry DMF. The flask was heated to 70−80 °C for 45 min, and a clear yellowish solution was formed. The reaction mixture was cooled to room temperature, and 30 mL of ethyl acetate, followed by 30 mL of petroleum ether, was added. A yellowish precipitate was formed and was washed with ethyl acetate. The solid was dried overnight in a vacuum. A 10 mL sample of 5% HCL (aq) was added to the dry solid, and the mixture was heated to ∼70−80 °C until a clear orange solution was formed (∼1−2 min). This clear solution was left at 4 °C for 72 h. The precipitate that was formed was washed with water and dried overnight in a vacuum to give 64 mg (0.08 mmole) of the product. Yield: 33%. The precipitate is the nearly pure product since the free hydrolyzed diethylenetriaminepentaacetic acid is soluble under these conditions.

FAB mass Calcd. for C34H34N4O14, 722.686; found, 720.980. ^{1}H NMR (250 MHz, DMSO:TFA, 50:1): 3.13−3.47 (broad, 9H); 3.88−4.01 (broad, 9H); 6.56−6.76 (m, 6H); 7.22 (t, 2H); 7.8(t, 1H).

Computer Modeling. All model building and energy minimizations were based on the SERCA1 crystal structures (Protein Database I. D. 1eul) and were performed with Discover and Insight II molecular modeling software version 2000 by MSI Inc., San Diego, CA. Energy minimizations (molecular mechanics) were performed with a medium dielectric constant of 4.0 and the consistent valence force field (cvff) provided with the software to an average absolute derivative of approximately 0.1 kcal mol^{-1} Å^{-1}. All side chains were simulated without formal charges. Partial charges for ATP were assigned by the builder module of the software and included 1.4, −0.5, −0.7, and −0.85 for all phosphorus atoms, the 5′ oxygen of the ribose ring, the phosphate bridging oxygen atoms, and the terminal oxygen atoms, respectively. Mg^{2+} was assigned a partial charge of 2.0.

To obtain a minimized structure for substrate bound conformations, the protein and ATP−Mg^{2+} were merged into a single structure and minimized together. The N domain of the Ca^{2+}-ATPase in $E_1 2Ca^{2+}$ (1eul) was severed from the P domain by deleting the peptide bonds between L356/T357 and K605/E606 in the apparent hinge region (*16*). ATP with the polyphosphate in extended conformation was then placed in the nucleotide binding pocket with the adenine ring in approximately the same position as that found for TNP−AMP (*8*). After energy minimization the N domain−ATP complex was rotated 80° until the γ phosphate overlaid D351. A search was conducted for a conformation of ATP−Mg^{2+}, which would simultaneously place Mg^{2+} next to D703 (the residue in a homologous position to those known to chelate Mg^{2+} in the HAD proteins), allow Mg^{2+} to complex α, β, and γ phosphate oxygens, and place the gamma phosphate between the Mg^{2+} and the side chain of D351. An appropriate conformation was selected from hexokinase (PDB ID 1qha) based on the bound form of AMP·PNP. The same conformation of ATP−Mg^{2+} was constructed and used to replace ATP by superimposing its adenine ring on that of the ATP in the minimized N domain·ATP complex. The amide bonds were then rejoined, and the whole structure was energy minimized to produce the models shown in Figures 6.

RESULTS

Cleavage Induced by the ATP−Fe^{2+} Complex in E_1 And E_2(K) Conformations. Figures 1 and 2 present data on cleavages mediated by the ATP−Fe^{2+} complex in the $E_1$3Na or E_1−P$(3Na)_{occ}$ states (left) and the $E_2(2Rb)_{occ}$ states (right). Cleavages mediated by ATP−Fe^{2+} in the E_1 state have been presented previously (*19*, *23*), Here we present similar data for comparison with fragments produced by ATP−Fe^{2+}-mediated cleavage in the E_2 state. Figure 1 also depicts known chymotryptic fragments of the α subunit (Chymo) (*40*) and Fe^{2+}-mediated cleavages in $E_1$3Na and $E_2(2Rb)_{occ}$ conformations (Cont Na and Cont Rb respectively), for comparison with mobilities of ATP−Fe^{2+}-mediated cleavage fragments. Fragments are identified exactly by N-terminal sequencing or are referred to as near the N-terminal sequences, as determined to within a few residues (about 10 or less in most cases) and described previously (*18*, *19*, *23*). Because we wished to compare cleavages induced by the

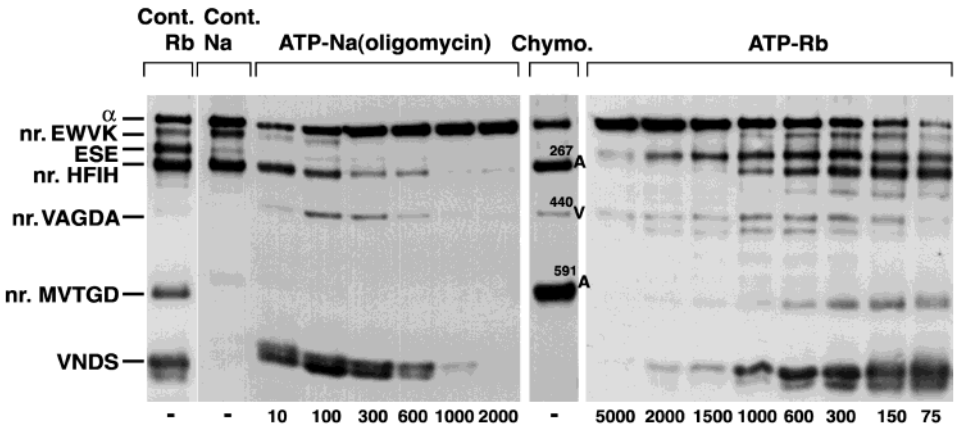

FIGURE 1: Cleavage of Na^+,K^+-ATPase mediated by the ATP−Fe^{2+} complex in E_1Na (or E_1−P) (left) or $E_2(Rb)$ conformations (right). (left) The cleavage (15′) was done in a medium containing 100 mM, NaCl, 5 μM Fe^{2+}, 5 mM ascorbate/H_2O_2, ATP(Tris) at the indicated concentrations (μM), and 50 μg/mL oligomycin (<0.5% ethanol). (right) The cleavage (15′) was done in a medium containing 100 mM RbCl, 75 μM Fe^{2+}, 5 mM ascorbate/H_2O_2, and ATP(Tris) at the indicated concentrations (μM). Cont. Na and Cont. Rb refer to control cleavage reactions in 100 mM NaCl or RbCl, respectively (3′), with 5 μM Fe^{2+} and 5 mM ascorbate/H_2O_2, in the absence of ATP. The central lane marked Chymo presents standard chymotryptic fragments denoted by their known N-terminal residues.

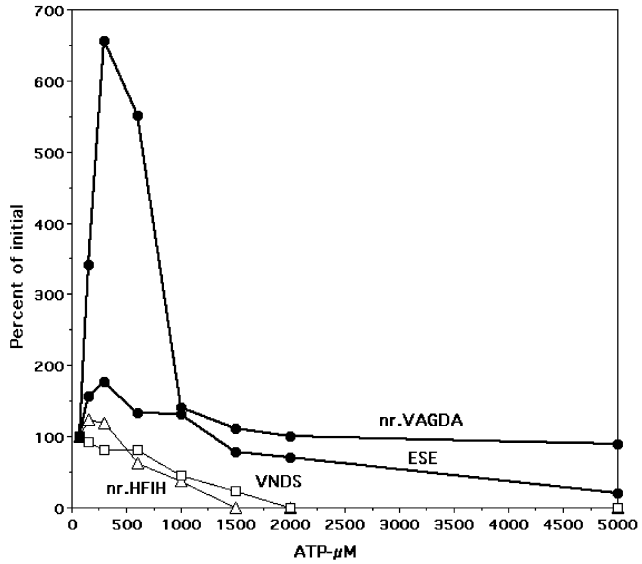

FIGURE 2: Quantification of fragments produced by ATP−Fe^{2+}-mediated cleavage in an $E_2(Rb)$ conformation. The immunoblot in Figure 1 (right) was scanned, and the intensity of each band was calculated in comparison to that at 75 μM ATP.

ATP−Fe^{2+} complex in Na^+- and Rb^+-containing media, the design of the experiment in Figure 1 (left) required the presence of ATP, Fe^{2+}, and Na^+ ions and also oligomycin. Under these conditions, Fe^{2+} ions substitute for Mg^{2+} ions, and the enzyme is phosphorylated, but oligomycin blocks the $E_1P \rightarrow E_2P$ conformational change and stabilizes the E_1P conformation (*41*, *19*). The pattern of fragments is identical in the E_1·3Na and E_1−P(3Na)occ states, as shown previously by comparing cleavage in the presence of the AMPPNP−Fe^{2+} complex (E_1·3Na) with that in ATP−Fe^{2+}, Na, and oligomycin (E_1−P(3Na)occ) conformation (*19*).

The cleavages induced in the E_1·3Na conformation, upon addition of increasing concentrations of ATP at a fixed concentration of Fe^{2+} ions (5 μM), include two prominent fragments at the 712VNDS position and a less prominent fragment referred to as near 440VAGDA (Figure 1, left). The experiment shows that this latter fragment has a electrophoretic mobility indistinguishable from that of a chymotryptic fragment with N-terminus 440 V (see also below). In parallel, fragments dependent on Fe^{2+} ions (near 80EWVK and near 283HFIH) are suppressed as the free Fe^{2+} is progressively bound by the ATP. As the total ATP concentration is raised far above that of the Fe^{2+} ions, all the cleavages are suppressed, due to competition between ATP and the ATP−Fe^{2+} complex (*19*, *23*). The fragment 712VNDS was found by sequencing to have N-terminus V712 (*19*). The fragment near 440VAGDA which runs parallel to the chymotryptic fragment has been shown recently by mass spectrometry to lie within 2−4 residues of V440 (see Discussion). The overall conclusion is that residues within the sequence 710GDVNDS (P domain), presumably D710, and near 440VAGDA (N domain) are in proximity when ATP−Fe^{2+} is bound in the $E_1$3Na conformation.

Figure 1 (right) depicts fragments produced by ATP−Fe-mediated cleavage in a Rb^+-containing medium ($E_2(Rb)_{occ}$ conformation). Since ATP is known to have a low affinity in the conformation $E_2(Rb)_{occ}$, (*1*, *2*), a rather high concentration of Fe^{2+} was used (75 μM), and the ATP concentration was varied from 75 to 5000 μM. Cleavages which appeared or were amplified upon raising the ATP must have been induced by binding of the ATP−Fe^{2+} complex. These could be distinguished from fragments caused by Fe^{2+} alone, the amplitude of which did not increase and was then reduced as the ATP concentration was raised, due to complexation of Fe^{2+} and removal of this ion from the protein. These latter fragments include the cleavage products near 283HFIH, near 608MVTGD, and 712VNDS. By contrast, the fragment ESE was amplified (compare 300 with 75 μMATP) before being suppressed at higher ATP concentrations, and two new but less prominent fragments, near 440VAGDA, appeared and were then also suppressed at high ATP. The differential effect of varying the ATP concentration on the ESE and near-440VAGDA fragments is visualized in Figure 2, which depicts the ratio of intensity of fragments at all ATP concentration compared to that at 75 μM. The ratio of the "near-VAGDA" fragments at 300 μM compared to 75 μM is large because the absolute amount of the fragments at 75 μM is low. Conversely, the relative increase of the ESE fragment is modest because this is a background fragment

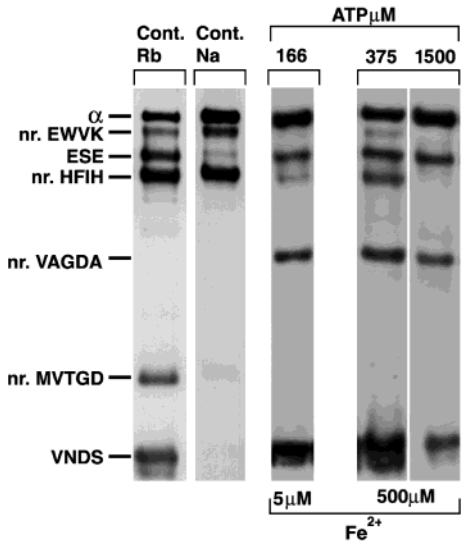

FIGURE 3: Cleavage of Na^+,K^+-ATPase mediated by high concentrations of ATP−Fe^{2+}. The cleavage (2′) was done in a medium containing 100 mM NaCl, 500 μM Fe^{2+} 5 mM ascorbate/H_2O_2, and 375 μm or 1500 μm ATP or 5 μM Fe^{2+} with 166 μMATP. The other controls are the same as those in Figure 1.

produced even without ATP. Suppression of the ESE and near-440VAGDA cleavages at very high ATP concentrations is, of course, attributed to competition between free ATP and the ATP−Fe^{2+} complex. Essentially identical results were observed when AMP−PNP replaced ATP (not shown). The upper of the two fragments marked as near 440VAGDA runs parallel to the chymotryptic fragment (N-terminus V440). The M_r values of the two fragments, based on known chymotryptic or Fe^{2+}-cleavage fragments for calibration (N-termini 214E, 267A, 440 V, 591A, and 712 V), are 66.3 and 63.0 kDa, respectively. Since the theoretical mass of the fragment with N-terminus 440 V is 64.16 kDa, the difference between the values 66.3 and 64.1 (2.2 kDa) represents an estimate of the error. From the estimated mass and error, the cleavage position of the smaller fragment can be calculated to lie between residues 460−490. Overall, the conclusion from the experiment is that the ATP−Fe^{2+} complex induced cleavages in both the A (212TGES) and N (near 440VAGDA and between 460 and 490) domains in the $E_2(2Rb)_{occ}$ conformation. Thus those sequences in the N and A domains are predicted to be in proximity in the $E_2(Rb)_{occ}$·ATP−Fe^{2+} conformation (see Discussion).[2]

Cleavages at High Concentrations of ATP−Fe^{2+}. Proposals that both high- and low-affinity ATP sites coexist in an E_1 conformation have been tested in a series of experiments, some of which are shown in Figure 3. If this concept is correct, one could expect to generate additional fragments at high concentrations of the ATP−Fe^{2+}, which should occupy both high- and low-affinity sites, by comparison with low concentrations of ATP−Fe^{2+} which occupy only high-affinity sites. The experiment in Figure 3 examined this question with ATP. In a medium containing Na^+ ions, 500 μM Fe^{2+}, and 375 or 1500 μM ATP (maximal ATP−Fe^{2+} concentrations of 375 or 500 μM, respectively), we observed formation of the near-440VAGDA and 712VNDS fragments, produced by cleavage of the E_1ATP−Fe^{2+} or E_1−P·Fe^{2+} complexes and the ESE fragment produced by cleavage of E_2−P·Fe^{2+}. With 375 μM ATP, minor amounts of the near-283HFIH and 80EWVK fragments attributable to uncomplexed Fe^{2+} ions also remained. The pattern of cleavages at 500 μM ATP−Fe^2 (1500 μM ATP plus 500 μM Fe^{2+}) is identical to that at 5 μm ATP−Fe^{2+} (166 μM ATP plus 5 μM Fe^{2+}). Experiments using other ATP analogues, including AMP−PNP, TNP-ATP, ATP-γ-S, and ATP-α-S, also produced the same fragments at the low and high concentrations of nucleotide−Fe^{2+} complex (not shown). In the latter cases, the ESE fragment was not observed because phosphorylation does not occur. Overall, the experiment of Figure 3 and all others using ATP analogues provide no evidence for appearance of additional fragments produced by binding of ATP−Fe^{2+} to a low-affinity site, in addition to those produced in the normal high-affinity site.

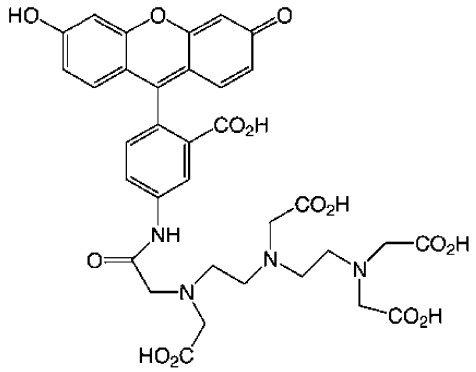

FIGURE 4: Fluorescein−DTPA.

Cleavages Induced by the Fluorescein−DTPA−Fe^{2+} Complex. Figures 4 shows the structure of a new derivative, fluorescein−DTPA, and Figure 5 describes specific oxidative cleavages mediated by the fluorescein−DPTA−Fe^{2+} complex. The DTPA moiety of the compound is a strong Fe^{2+} chelator (Ka $10^{16.5}$) (*42*), and the chelated Fe^{2+} is known to generate OH radicals in the presence of ascorbate plus hydrogen peroxide (*43*). It was thought that the fluorescein moiety could direct the compound to the nucleotide binding site, as in the case of FITC (*37*), and the bound Fe^{2+} chelate could mediate specific cleavages in the site. Since fluorescein−DTPA−Fe^{2+} and ATP−Fe^{2+} are Fe^{2+} chelators with a quite different structure, they might be expected to produce different cleavage fragments. Surprisingly, however, the fluorescein−DTPA−Fe^{2+} complex mediated similar cleavages to the ATP−Fe^{2+} complex.

The experiment of Figure 5(A) was done in a Na^+-containing medium ($E_1$3Na conformation) with a fixed Fe^{2+} concentration (50 μM) and increasing fluorescein−DTPA concentrations (100−500 μM). Fluorescein−DTPA (100 μM) suppressed the fragments near 80EWVK and 283HFIH mediated by uncomplexed Fe^{2+} and induced new cleavages near 440VAGDA and 712VNDS positions. The latter were also suppressed at high concentrations of fluorescein−DTPA

[2] Due to the small amounts of the near VAGDA fragments produced, one might hypothesise that, in the Rb-medium, ATP stabilizes small amounts of the E_1 conformation, which is then cleaved at the near VAGDA positions as in Figure 1. However, since the peak amounts of the near VAGDA fragments produced in the Na and Rb media are about equal (compare Figure 1 right and left), that supposition would require that most of the enzyme is converted to the E_1·ATP form in the Rb medium.This cannot be correct because the amount of the VNDS fragment, the major representative of cleavages in E1, is not amplified but decreases monotonically as ATP concentration is raised. Thus, the near-VGADA fragments appear to be bona fide cleavages of the E_2(Rb) conformation.

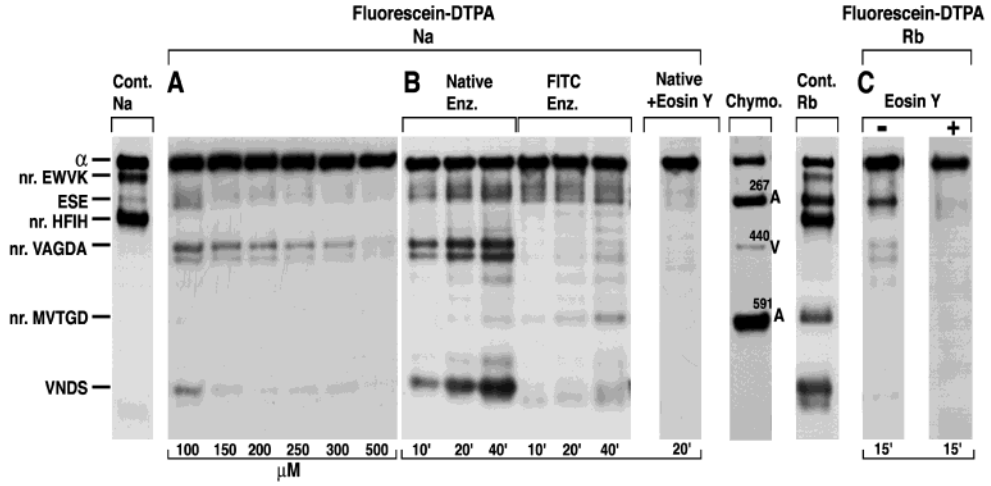

FIGURE 5: Specific oxidative cleavages mediated by the fluorescein−DTPA−Fe^{2+} complex. (A) The cleavage (20′) was done in a medium containing 100 mM NaCl, 50 μM Fe^{2+}, 10 mM ascorbate/H_2O_2, and indicated concentrations of fluorescein−DPTA (μM). Other controls are the same as those in Figure 1. (B) The cleavage was done in a medium 100 mM NaCl, 70 μM Fe^{2+}, 20 mM ascorbate, 10 mM H_2O_2, and 200 μM fluorescein−DTPA for the indicated time in minutes. FITC enzyme refers to enzyme pretreated with FITC. Native + eosin Y depicts the result of cleavage (20′) in the presence of 30 μM eosin Y. (C) Cleavage (20′) was done in a medium containing 150 mM Rb, 70 μM Fe^{2+}, 20 mM ascorbate, 10 mM H_2O_2, and 150 μM fluorescein−DPTA, without or with 125 μM eosin Y. Other controls are the same as those in Figure 1.

(500 μM). Suppression at the higher fluorescein−DTPA concentration is consistent with competition between free and Fe^{2+}-complexed fluorescein−DTPA in the binding site, as is the case for competition between free ATP and the ATP−Fe complex (see Figure 1). A time course of appearance of fragments induced by fluorescein−DPTA−Fe^{2+} Figure 5(B) shows that there are differences in intensity of cleavages compared to ATP−Fe-mediated cleavages. Specifically, fluorescein−DTPA-mediated cleavages produced two bands near 440VAGDA, the upper one being more prominent than the 712VNDS fragment. The 214ESE band seen with ATP−Fe^{2+} does not appear with fluorescein−DTPA because phosphorylation cannot occur. ATP−Fe^{2+}-mediated cleavage produces mainly the upper of the two fragments near 440VAGDA and at a lower intensity compared to that of the major 712VNDS fragment. Nevertheless, the electrophoretic mobility of the fragments is not different in the two cases. (In a choline chloride-containing medium, E_1, ATP−Fe^{2+}-mediated cleavage produces both of the bands near 440VAGDA; *19*). The Mr of these two bands produced with fuorescein−DTPA−Fe^{2+} were estimated to be 66 and 63 kDa, respectively, essentially identical to that of the fragments produced with ATP−Fe^{2+}. A number of experiments were carried out to verify the selectivity and site-specific mechanism of cleavages mediated by fluorescein−DTPA. One criterion is displacement of the reagent by ATP itself. At low concentrations of ATP, suppression of the cleavage was observed, but the experiment is complicated by the fact that as the ATP concentration is raised, the ATP−Fe^{2+} complex itself induces cleavages (not shown). Alternatively, one can use FITC, which covalently modifies Lys501 and prevents ATP binding (*37*, *44*), and eosin Y, which competes with ATP for the binding site with a high affinity (*45*). As seen in Figure 5B, the fluorescein−DTPA-induced cleavages near 440VAGDA and at 712VNDS in the Na^+ medium were completely suppressed in FITC-modified enzyme or in the presence of eosin Y, confirming that fluorescein−DTPA−Fe^{2+} is bound within the nucleotide pocket. The two right-hand lanes of the gel, Figure 5C, depict cleavages induced by fluorescein−DTPA in a Rb^+-containing medium. The experiment uses a fluorescein−DTPA concentration high enough to complex all free Fe^{2+} and suppresses the standard Fe^{2+}-mediated cleavages (seen in Cont. Rb). Under this condition, observed fragments are the product only of fluorescein−DPTA−Fe^{2+} complex-mediated cleavage. The result shows a prominent band at the ESE position and two minor bands in the near-440VAGDA positions, as found also for ATP−Fe^{2+} in a Rb^+-containing medium (Figure 1). In the presence of eosin Y, the fragments were not observed, indicating again that cleavage depends on binding in the nucleotide site in the E_2 conformation.

DISCUSSION

Locating Cleavage Positions by Mass Spectrometry. Previously, the locations of cleavages for fragments which could not be sequenced directly was estimated approximately to within about 10 residues (*18*, *19*, *23*). Recently a significant improvement has been achieved for fragments generated by ATP−Fe^{2+}-mediated cleavage using MALDI-TOF mass spectrometry after electroelution from gels. A preliminary communication has been sent for publication (Goldshleger et al., 2002), and a full manuscript is in preparation (Shainkaya, A., Goldshleger, R., and Karlish, S. J. D., unpublished work).

The mass of the intact pig kidney α subunit was found to be 112 198.9 ± 491 kDa ($n = 4$), compared to the theoretical mass of 112 281 kDa. The predicted masses of the known fragment 712VNDS C-terminus, produced by ATP−Fe-mediated cleavage, and its complementary fragment with N-terminus 712VNDS are 34 552 and 77 747 Da, respectively. The masses estimated by MALDI-TOF were found to be 34 806 ± 97 ($n = 7$) and 78 083 Da, respectively. The error of the measurements of these known masses equals approximately five residues for the intact α subunit, and the position of the cleavage producing the VNDS fragment is accurate to within three residues. These measurements provide a yardstick by which to gauge the accuracy of the masses of unknown fragments.

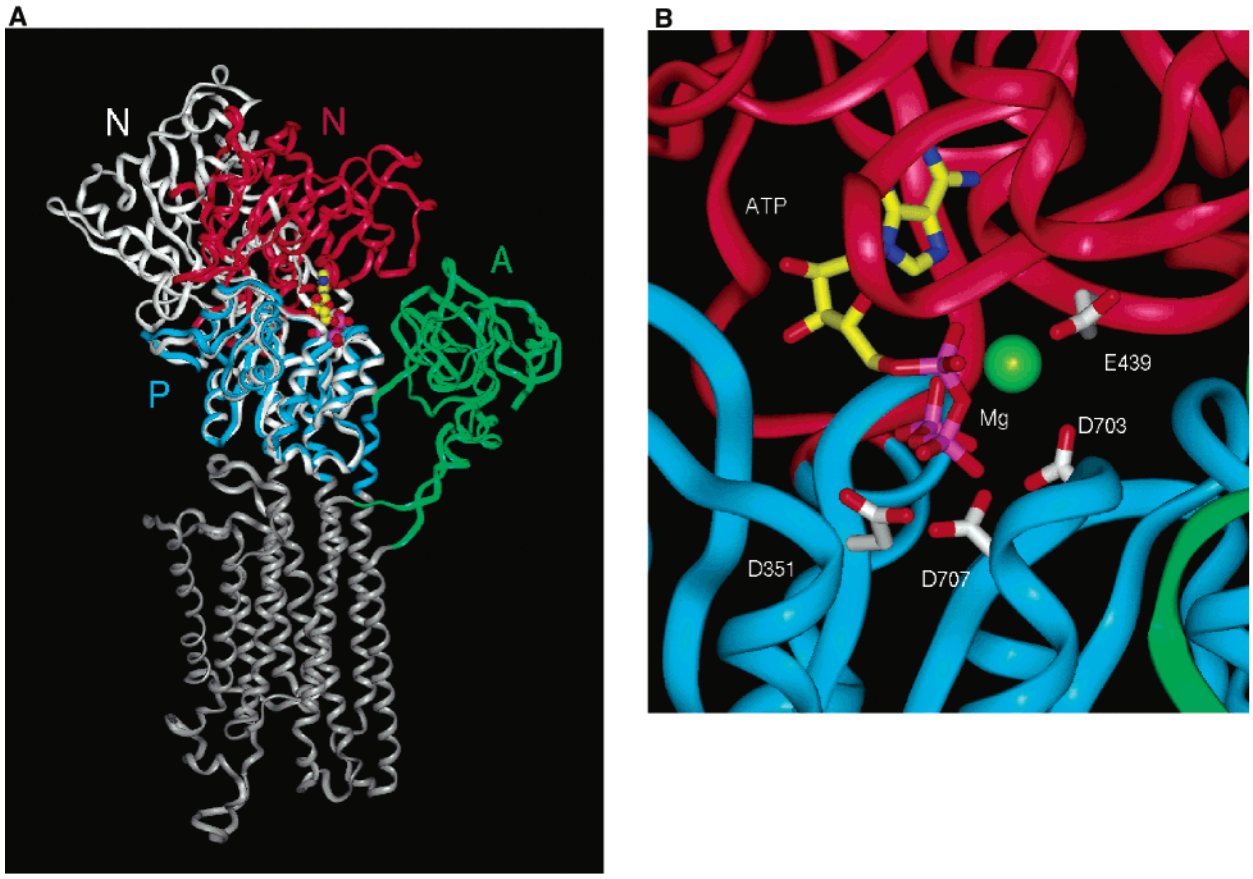

FIGURE 6: Model of Ca^{2+}-ATPase in an E_1·ATP−Mg^{2+} conformation. The 1EUL·pdb structure is depicted in white. The tilted N domain is red, and P and A domains are blue and green, respectively. (A) Long range and (B) close up. For modeling procedures, see Experimental Methods. In the view of the molecule in Figure 6B chosen to depict proximity of the Mg^{2+} ion to D703 and D439, the Mg^{2+} ion appears to be closest to the αP of ATP. The actual distances of closest approach of the Mg ions are as follows: γP, 2.82A; βP, 4.2A; αP, 3.0A.

The mass of the upper of the two bands referred to as near-440VAGDA and that of its N-terminal complementary fragment were found to be 64 435 Da and 48 571 Da, respectively The predicted masses of the chymotryptic fragments C-terminus V440 and N-terminus V440 are 64 231 and 48 069 Da, respectively. The differences between measured and predicted masses are between 2 and 4 residues, which is within the error for the estimates of known fragments. Therefore, the cleavage position of the near-440VAGDA fragment must lie within 2−4 residues of V440. By comparison with the inference based on a similar electrophoretic mobility to the chymotryptic fragment with N-terminus 440 V, which has an uncertainty of about 10 residues, this measurement significantly improves the accuracy in the assignment of the position of cleavage. The unknown fragment referred to as near-214ESE and its complementary N-terminal fragment, which are the major cleavage products in conditions of phosphorylation, were found to have masses of 89.687 and 23 275 ± 62 Da (n = 7), compared to the theoretical masses of 88 852 (C-terminus 214E) and 23 449 Da (N-terminus 214ESE), respectively.

An important point from these MALDI-TOF MS measurements is that the accuracy is sufficient to justify the molecular modeling of proximity of the 712VNDS and near-440VAGDA sequences, as described in the next paragraph.

Testing Predictions of Cleavage Experiments with Molecular Models. It has been clear that the N and P domains must approach each other in order to allow the γP of ATP to come into contact with and phosphorylate D369 in the P domain, while the purine moiety is docked in the N domain (*8*, *47*). The predicted proximity of D710 (P domain) and a residue near or within the sequence 440VAGDA (N domain), based on cleavage by ATP−Fe complex in the E_1 conformation Figure 1, provides a testable constraint for modeling this N to P closure.

We have constructed a model of the SERCA Ca^{2+}-ATPase in an E_1·ATP·Mg^{2+} conformation as a paradigm for interpreting the Na^+,K^+-ATPase cleavage results (Figure 6). This involves tilting the N toward the P domain by about 80° and rotation about peptide bonds between L356/T357 and K605/E606 in the small segments connecting the domains (see Methods). A similar procedure involving a solid body movement, but without ATP−Mg^{2+} docked, has been described recently (*16*). In the α-subunit of Na^+,K^+-ATPase, 440VAGDASE is homologous to 436KVGEATE of Ca^{2+}-ATPase. Numbering of residues in the models is that of SERCA, while numbers of the homologous residues of Na,K-ATPase are given in parentheses. As seen in Figure 6, with the modeling constraints described in the Methods, D703 (D710 in Na,K-ATPase) indeed comes within 4.4 Å of E439 (D443 in Na,K-ATPase), and both residues are 3−3.2 Å distant from the Mg^{2+} ion. This is compatible with a direct role of both residues in Mg^{2+} ligation. D710 has been shown by mutations to play a crucial role in Mg^{2+} binding in the E_1 conformation (*49*). The modeling suggests that D443 is a candidate Mg^{2+} binding residue, but on the basis of the

cleavages, this should be less prominent than that of D710. A role for D443 in Mg^{2+} binding must be tested independently by mutations, particularly since a negatively charged residue is found in most but not all P-type pumps at this position. D707 (D714 in Na,K-ATPase) is 6.5 Å from the Mg^{2+} and could interact via a shared water molecule. Binding to D714 as well as to D710 could explain the finding that the 712VNDS cleavage produces two closely running fragments, only the upper one of which has V712 as the N-terminus (*19*). The assigned role of D710, and a possible involvement of D714 via a water molecule, fits with the known role of homologous aspartates in the HAD superfamily, including phosphoserine phosphatase and phosphonatase, for which crystal structures with bound Mg^{2+} ions are available (*26*−*28*). T353 (T371 in Na,K-ATPase) has been suggested to interact with the Mg^{2+} ion (*48*) and is close to the Mg^{2+} ion, at a distance of 4.5 Å

Cleavages in the E_2(Rb)occ conformation mediated by the ATP−Fe^{2+} or fluorescein−DTPA−Fe^{2+} complexes suggest close proximity within the 212TGES sequence (A domain) and residues near 440VAGDA and between 460 and 490 (N domain). The predicted proximity between 212TGES and 440VAGDA can be tested by reference to the E_2 model (PDB ID 1kju). This model shows that E439 of Ca^{2+}-ATPase (D443 of Na^+,K^+-ATPase) is indeed located within 4.3 Å of S186 (P217 in Na,K-ATPase), close to the 181TGES sequence, or 3.3 Å of R174 (K205 in Na,K-ATPase) located in the same loop. The sequence 460−490 corresponds to residues 471−497 in Ca^{2+}-ATPase, which includes F487 (F475 in Na,K-ATPase), R489, and K492 (K480 in Na,K-ATPase), thought to participate in ATP binding (*50*). In the SERCA structure, the loop containing residues 471−497 is located proximal to the loop containing the 439EATE sequence. However, the cleavage position, within 460−490 of Na,K-ATPase is not known accurately enough to produce a detailed prediction of sequence proximity.

The Fluorescein−DTPA−Fe Complex as a Cleavage Agent. Since the specificity of cleavages mediated by bound fluorescein−DTPA−Fe^{2+} in both E_1Na and E_2(Rb) conformations is similar to that for bound ATP−Fe^{2+}, albeit with quantitative differences in the intensity of the different fragments, the conclusions concerning the domain and sequence proximities are, of course, similar. Because the structures of ATP−Fe^{2+} and fluorescein−DTPA−Fe^{2+} are different, the similar selectivity of the cleavages has the important mechanistic implication that both reagents direct the Fe^{2+} to the same locations on the protein and that cleavages occur only next to residues which bind the Fe^{2+} directly. Conversely, bonds next to residues which do not bind the Fe^{2+} would not be predicted to undergo cleavage, even if they are in proximity.

Functional Interactions of ATP and Mg Ions in the Catalytic Site. Figure 7 depicts schematic models of Mg^{2+} and ATP binding sites in the four major conformations of the catalytic cycle, $E_1$3Na,ATP.Mg^{2+}, E_1−P(3Na)occ, E_2−P, and E_2(2K)occ·ATP·Mg^{2+}. In E_1 and E_1P conformations, the N and P domains interact, and the A domain is displaced to the side, while in E_2P and E_2K conformations, the A domain interacts with both N and P domains, thus hindering the N to P interaction.

(A) Mg^{2+} Sites. In the $E_1$3Na,ATP·Mg^{2+} conformation, Mg^{2+} is depicted as being ligated to both D710 and, as we propose, to D443, Figure 6. In E_1−P the Fe-catalyzed cleavages are the same as in E_1, and so it is assumed that Mg^{2+} (Fe^{2+}) binding is the same in the two states.

Upon phosphorylation and conversion of E_1−P to E_2−P, a change occurs in ligation of the Mg^{2+} ion (*18*, *19*, *23*). The major cleavage, and presumably the closest binding, occurs within the 212TGES sequence, while that in the 712VNDS sequence is less prominent. This is indicative of the A to P interaction. The cleavage near 440VAGDA is not seen in E_2−P, indicating that the N to P interaction is absent (*19*). As discussed previously, the change in Mg^{2+} ligation from D710 to the 212TGES sequence must create a different geometry of ligands surrounding bound phosphate (*20*), and together with a more hydrophobic environment, this may be crucial for inducing reactivity of E_2−P to water, as compared to the ADP sensitivity of E_1−P. Upon hydrolysis of E_2−P, the tightly bound Mg^{2+} ions dissociate (*19*, *25*).

Upon rebinding of the substrate ATP−Mg^{2+} to the E_2(K) conformation, the Mg^{2+} ions appear to be directed to residues in the N and A domains (near 212TGES (A), 440VAGDA, and presumably within sequence 460−490 (N)), as suggested by the cleavage experiments and modeling. Following the E_2(K) → E_1Na transition to the high ATP affinity conformation, the Mg^{2+} ion is re-bound to the D710 (and perhaps D714), which prepares the ATP molecule for the next round of phosphorylation.

(B) ATP Sites. ATP binds to the E_2(K) conformation with low affinity and greatly accelerates its transition to the E_1 conformation which binds ATP with high affinity (*1*, *2*). The structural models of E_1ATP·Mg^{2+} and the E_2 form offer a possible explanation for the different ATP affinities of the two conformations and acceleration by ATP of E_2(K) → E_1.

A detailed view of the ATP−Mg^{2+} site in the E_1·ATP−Mg^{2+} model reveals the contact residues of the docked ATP−Mg^{2+} molecule, several of which (K515, T441, F487, R489, K492) are already known to be involved in ATP binding (*8*). For Na^+,K^+-ATPase, residues K501 (K515), G502 (G516), and K480 (K492) have been shown to be important by labeling methods (*51*−*54*) and R544 (R560) by mutagenesis (*55*). In the Ca^{2+}-ATPase model, the β and γ phosphates of ATP interact with T353 and K684 (*48*). Thus, multiple favorable contacts surrounding ATP in both N and P domains account for high-affinity ATP binding. The interaction of the phosphates with the Mg^{2+} bound to D703 further stabilizes the bound ATP−Mg^{2+} complex (*55*).

The low ATP affinity in E_2 conformations can be explained, at least in part, by the lack of accessibility to D351, D703, D707, T353, and K684 side chains within the P domain when these residues are completely overlaid by the A domain. In the E_2 model, E183 in the A domain appears to provide key contacts to the P domain by H-bonding to D351, T353, K352, T625, and G626. Thus, whereas the adenine and ribose binding pocket appears to be still accessible in E_2, the Mg^{2+} and polyphosphate groups are forced to contact other residues within 181TGESVSV and 436KVGEATET, where the binding energy is not as great. In essence, stabilization of E_1 by ATP can be understood as a result of competition between the ATP and the A domain for contact residues in the P and N domains. This concept can also explain acceleration by ATP of the slow E_2(K) → E_1 conformational transition. Assuming that the activation energy of E_2(K) → E_1 without ATP is dictated

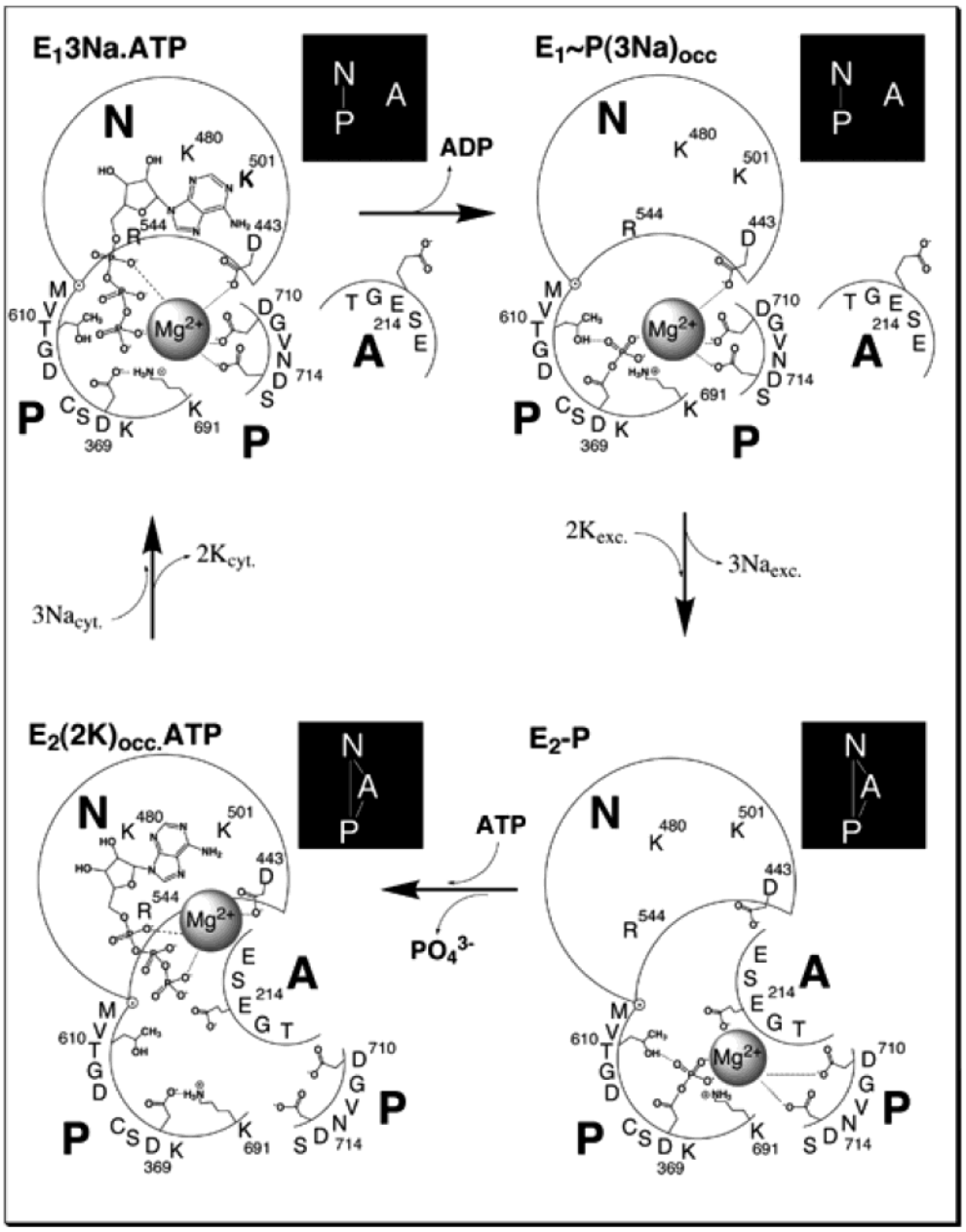

FIGURE 7: Schematic diagrams of N, P, and A interactions and ATP−Mg^{2+} or Mg^{2+} binding sites in the different states of the catalytic cycle. The proposed role for D443 in Mg binding is based on the cleavage plus modeling data and is still hypothetical at this stage.

mainly by breaking of A to N and A to P interactions, binding of ATP to E_2(K) should reduce the activation energy by competing with the A domain for the residues R560 (N), K352, and T353 (P) and repelling the negative groups of E183 (A) responsible for the A to P interaction. By contrast, the rapid $E_1 \rightarrow E_2$(K) transition is not affected by ATP (*56*). Presumably, the activation energy of the $E_1 \rightarrow E_2$(K) transition is dictated primarily by breaking of bonds preempted by the movement of the A domain toward the P and N domains. Breaking these bonds should not be affected by binding of ATP in the N and P domain.

(C) One or Two ATP Sites? The hypothesis that Na^+,K^+-ATPase has two ATP sites located either on the same α/β protomer or on interacting protomers is a controversial topic (see ref *31* for a review favoring the oligomer hypothesis). The minimal functional unit in detergent solution is unequivocally an α/β protomer (*57*, *58*), and in our view, the results presented here support other recent findings (*59*, *60*) which favor a single ATP site mechanism.

The evidence from the Ca^{2+}-ATPase structure is clear-cut in that only one ATP binding pocket can be discerned (*8*). The assumption of a similar structure of the ATP binding domain of Ca^{2+}-ATPase and Na^+,K^+-ATPase is justified by the homologies in the N domain and evidence that several homologous residues are involved in ATP binding in both the Ca^{2+}-ATPase and Na^+,K^+-ATPase (K515, K480, R544 etc.). If the explanation given above for the difference of ATP affinities in the two conformations, based on the $E_1ATP{\cdot}Mg^{2+}$ and E_2 models, is correct, there is no need to invoke separate high- and low-affinity binding pockets. The observation that the same fragments were observed at both high and low concentrations of ATP−Fe^{2+} (and several other ATP analogues), Figure 3, implies that there is only one ATP site in the E_1 conformation. Although lack of detectable

cleavages from a low-affinity site is not rigorous proof against its existence, the observation of specific cleavages mediated at a low-affinity ATP−Fe^{2+} site in the E_2(Rb) conformation (Figure 1) suggests that if a low-affinity site existed in the E_1 conformation it would have been detected. The concept of interacting protomers in a dimeric or tetrameric complex (*31*−*33*) requires that that E_1 and E_2 forms are simultaneously present in the two halves of the oligomer, at least in the presence of ATP−Mg^{2+}. The distinct patterns of oxidative cleavage mediated by ATP−Fe^{2+} in the Na^+-containing and Rb^+-containing media do not fit this concept.

CONCLUSION AND PERSPECTIVE

This work illustrates the advantage of combining ATP−Fe^{2+}-mediated cleavages with molecular modeling to infer properties of the energy transduction mechanism not observable from the Ca-ATPase crystal structure itself. Specific predictions on possible roles of different residues in Mg^{2+} binding (D369, D710, D443,) are now being tested directly by looking at Fe^{2+}- and ATP−Fe^{2+}-mediated cleavage of Na,K-ATPase expressed in the yeast *Pichia pastoris* (Strugatsky, D., and Karlish, S. J. D., unpublished work).

ACKNOWLEDGMENT

We are grateful to Dr. R. L. Post for invaluable comments on the manuscript.

REFERENCES

1. Glynn, I. M., and Karlish, S. J. D. (1990) *Annu. Rev. Biochem. 59*, 171−205.
2. Glynn, I. M. (1993) *J. Physiol. (London) 462*, 1−30.
3. Moller, J. V., Juul, B., and le Maire, M. (1996) *Biochim. Biophys. Acta 1286*, 1−51.
4. Lutsenko, S., and Kaplan, J. H. (1995) *Biochemistry 34*, 15607−15613.
5. Therien, A. G., Pu, H. X., Karlish, S. J. D., and Blostein, R (2001) *J. Bioenerg. Biomembr. 33*. 407−414.
6. Fambrough, D. M., Lemas, M. V., Hamrick, M., Emerickm M., Renaud, K. J., Inman, E. M., Hwang, B., and Takeyasu, K. Am (1994) *Am. J. Physiol. 266*, C579−589.
7. Geering, K. (2001) *J. Bioenerg. Biomembr. 33*, 425−438.
8. Toyoshima C., Nakasako, M., Nomura, H., and Ogawa, H. (2000) *Nature 405*, 647−655.
9. Axelsen, K. B., and Palmgren, M. G. (1998) *J. Mol. Evol. 46*, 84−101.
10. Sweadner, K. J., and Donnet, C. (2001) *Biochem. J. 356*, 685−704.
11. Rice, W. J., Young, H. S., Martin, D. W., Sachs, J. R., and Stokes, D. L. (2001) *Biophys. J. 80*, 2187−2197.
12. Hebert, H., Purhonen, P., Vorum, H., Thomsen, K., and Maunsbach, A. B. (2001) *J. Mol. Biol. 314*, 479−494.
13. Aravind, L., Galperin, M. Y., and Koonin, E. V. (1998) *Trends Biochem. Sci. 23*, 127−129.
14. Ridder, I. S., and Dijkstra, B. W. (1999) *Biochem. J. 339*, 223−226.
15. Ogawa, H., Stokes, D. L., Sasabe, H., and Toyoshima, C. (1998) *Biophys. J. 75*, 41−52.
16. Xu, C., Rice, W. J., He, W., and Stokes, D. L. (2002) *J. Mol. Biol. 61*, 884−894.
17. Goldshleger, R., and Karlish, S. J. D. (1997) *Proc. Natl. Acad. Sci. U.S.A. 94*, 9596−9601.
18. Goldshleger, R., and Karlish, S. J. D. (1999) *J. Biol. Chem. 274*, 16213−16221.
19. Patchornik, G., Goldshleger, R., and Karlish, S. J. D. (2000) *Proc. Natl. Acad. Sci. U.S.A. 97*, 11954−11959.
20. Goldshleger, R., Patchornik, G., Bar Shimon, M., Tal, D. M., Post, R. L., and Karlish, S. J. D. (2001) *J. Bioenerg. Biomembr. 33*, 387−399.
21. Bar Shimon, M., Goldshleger, R., and Karlish, S. J. D. (1998) *J. Biol. Chem. 273*, 34190−34195.
22. Tal, D. M., Capasso, J. M., Munson, K., and Karlish, S. J. D. (2001) *Biochemistry 40*, 12505−12514.
23. Shin, J. M., Goldshleger, R., Munson, K. B., Sachs, G., and Karlish, S. J. D. (2001) *J. Biol. Chem. 276*, 48440−48450.
24. Rendi, R., and Uhr, M. L. (1964) *Biochim. Biophys. Acta 89*, 520−531.
25. Fukushima, Y., and Post, R. L. (1978) *J. Biol. Chem. 253*, 6853−6872.
26. Wang, W., Kim, R., Jancarik, J., Yokota, H., and Kim, S. H. (2001) *Struct. Folding Des. 9*, 65−72.
27. Chi, H., Wang, W., Kim, R., Yokota, H., Damo, S., Kim, S.-H., Wemmer, D., Kustu, S., and Yan, D. (2001) *Proc. Natl. Acad. Sci. U.S.A. 98*, 8525−8530.
28. Morais, M. C., Zhang, W., Baker, A. S., Zhang, G., Dunaway-Mariano, D., and Allen, K. N. (2000) *Biochemistry 39*, 10385−10396.
29. Karlish, S. J. D., and Yates, D. (1978) *Biochim. Biophys. Acta 527*, 115−130.
30. Lüpfert, C., Grell, E., Pintschovius, V., Apell, H. J., Cornelius, F., and Clarke, R. J. (2001) *Biophys. J. 81*, 2069−2081.
31. Taniguchi, K., Kaya, S., Abe, K., and Mardh, S. (2001) *J. Biochem. (Tokyo) 129*, 335−342.
32. Thoenges, D., Amler, E., Eckert, T., and Schoner, W. (1999) *J. Biol. Chem. 274*, 1971−1978.
33. Linnertz, H., Urbanova, P., Obsil, T., Herman, P., Amler, E., and Schoner, W. (1998) *J. Biol. Chem. 273*, 28813−28821.
34. Ward, D. G., and Cavieres, J. D. (1996) *J. Biol. Chem. 271*, 12317−12321.
35. Ward, D. G., and Caviere, J. D. (1998) *J. Biol. Chem. 273*, 33759−65.
36. Jørgensen, P. L. (1988) *Methods Enzymol. 156*, 29−43.
37. Karlish, S. J. D. (1980) *J. Bioenerg. Biomembr. 12*, 111−135.
38. Schägger, H., and von Jagow, G. (1991) *Anal. Biochem. 199*, 223−231.
39. Capasso, J. M., Hoving, S., Tal, D. M., Goldshleger, R., and Karlish, S. J. D. (1992) *J. Biol. Chem. 267*, 1150−1158.
40. Jorgensen, P, L., and Andersen, J, P. (1988) *J. Membr. Biol. 103*, 95−120.
41. Fahn, S., Koval, G. J., and Albers, R. W. (1966) *J. Biol. Chem. 241*, 1882−1889.
42. Martell, A. E., and Smith, R. M. (1974) in *Critical Stability Constants*, pp 281−285, Plenum Press, New York.
43. Floyd, R. A. (1982) *Can. J. Chem. 60*, 1577−1586.
44. Farley, R. A., Tran, C. M., Carilli, C. T., Hawke, D., and Shively, J. E. (1984) *J. Biol. Chem. 259*, 9532−9635.
45. Skou, J. C., and Esmann, M. (1981) *Biochim. Biophys. Acta 647*, 232−240.
46. Goldshleger, R., Pachornik, G., Mehlman, T., Benjamin, M., Merhav, D., Karlish, S. J. D., and Shainskaya, A. (2002) *Proceedings of the 50th Annual Meeting of the American Society of Mass Spectrometry*, Orlando, Florida, June 2−6.
47. Maclennan, D. H., and Green, N. M. (2000) *Nature 405*, 633−634.
48. Clausen, J. D., McIntosh, D. B., Woolley, D. G., and Andersen, J. P. (2001) *J. Biol. Chem. 276*, 35741−35750.
49. Pedersen, P. A., Jorgensen, J. R., and Jorgensen P. L (2000) *J. Biol. Chem. 275*, 37588−37595.
50. McIntosh, D. B., Woolley, D. G., Vilsen, B., and Andersen, J. P. (1996) *J. Biol. Chem. 271*, 25778−25789.
51. Farley, R. A., Tran, C. M., Carilli, C. T., Hawke, D., and Shively, J. E. (1984) *J. Biol. Chem. 259*, 9532−9635.
52. Tran, C. M., Huston, E. E., and Farley, R. A. (1994) *J. Biol. Chem. 269*, 6558−6565.
53. Hinz, H. R., and Kirley, T. L. (1990) *J. Biol. Chem. 265*, 10260−10265.
54. Tran, C. M., Scheiner-Bobis, G., Schoner, W., and Farley, R. A. (1994) *Biochemistry 33*, 4140−4147.
55. Jacobsen, M. D., Pedersen, P. A., and Jorgensen, P. L. (2002) *Biochemistry 41*, 1451−1456.
56. Steinberg, M., and Karlish, S. J. D. (1989) *J. Biol. Chem. 264*, 2726−2734.
57. Brotherus, J. R., Jacobsen, L., and Jorgensen, P. L. (1983) *Biochim. Biophys. Acta 731*, 290−303.
58. Ward, D. G., and Cavieres, J. D. (1993) *Proc. Natl. Acad. Sci. U.S.A. 90*, 5332−5336.
59. Martin, D. W., and Sachs, J. R. (2000) *J. Biol. Chem. 275*, 24512−24517.
60. Martin, D. W., Marecek, J., Scarlata, S., and Sachs, J. R. (2000) *Proc. Natl. Acad. Sci. U.S.A. 97*, 3195−3200.

BI026334D